Superthreshold Behavior of Ultrasound-Induced Lung Hemorrhage in Adult Rats

Role of Pulse Repetition Frequency and Pulse Duration

William D. O'Brien, Jr, PhD, Douglas G. Simpson, PhD, Leon A. Frizzell, PhD, James F. Zachary, DVM, PhD

Objective. The purpose of this study was to enhance the findings of an earlier ultrasound-induced lung hemorrhage study (Ultrasound Med Biol 2003; 29:1625–1634) that estimated pressure thresholds as a function of pulse duration (PD: 1.3, 4.4, 8.2, and 11.6 μs; 2.8 MHz; 10-s exposure duration [ED]; 1-kHz pulse repetition frequency [PRF]). In this study, the roles of PRF and PD were evaluated at 5.9 MPa, the peak rarefactional pressure threshold near that of the ED_{50} estimate previously determined. ***Methods.*** A 4 × 4 factorial design study (PRF: 50, 170, 500, and 1700 Hz; PD: 1.3, 4.4, 8.2, and 11.6 μs) was conducted (2.8 MHz; 10-s ED). Sprague Dawley rats (n = 175) were divided into 16 exposure groups (10 rats per group) and 1 sham group (15 rats); no lesions were produced in the sham group. Logistic regression analysis evaluated significance of effects for lesion occurrence, and Gaussian tobit analysis evaluated significance for lesion depth and surface area. ***Results.*** For lesion occurrence and sizes, the main effect of PRF was not significant. The interaction term, PRF × PD, was highly significant, indicating a strong positive dependence of lesion occurrence on the duty factor. The main effect of PD was almost significant ($P = .052$) and thus was included in the analysis model for a better fit. ***Conclusions.*** Compared with the findings from a PRF × ED factorial study (J Ultrasound Med 2005; 24:339–348), a function that considers PRF, PD, and ED might yield a sensitive indicator for consideration of a modified mechanical index, at least for the lung. ***Key Words:*** duty factor; lung hemorrhage; pulsed ultrasound; pulse duration; pulse repetition frequency; rat lung; ultrasound bioeffects.

Abbreviations
ED, exposure duration; FDA, Food and Drug Administration; MI, mechanical index; p_c, peak compressional pressure; PD, pulse duration; PRF, pulse repetition frequency; p_r, peak rarefactional pressure

Received November 4, 2005, from the Bioacoustics Research Laboratory, Department of Electrical and Computer Engineering (W.D.O., L.A.F.), and Department of Pathobiology (J.F.Z.), University of Illinois, Urbana, Illinois USA; and Department of Statistics, University of Illinois, Champaign, Illinois USA (D.G.S.). Revision requested December 19, 2005. Revised manuscript accepted for publication March 1, 2006.

We thank J. P. Blue, R. J. Miller, and K. Norrell for conducting the experiments so reliably; Y. Yang for providing the statistical analyses; and J. Christoff, O. Coffield, T. Fong, B. McNeill, R. Patel, S. Sakai, R. Towa, A. Tevar, and B. Zierfuss for technical assistance. This work was supported by National Institutes of Health grant EB02641 (formerly HL58218), awarded to W.D.O. and J.F.Z., and National Science Foundation grant DMS-0073044, awarded to D.G.S.

Address correspondence to William D. O'Brien, Jr, PhD, Bioacoustics Research Laboratory, Department of Electrical and Computer Engineering, University of Illinois, 405 N Mathews, Urbana, IL 61801 USA.
E-mail: wdo@uiuc.edu

Ultrasound-induced lung hemorrhage is a well-documented in vivo bioeffect in mice,[1–12] rats,[11–20] monkeys,[21] rabbits,[7,8] and pigs.[7,8,22–25] Acoustic pressure lung hemorrhage thresholds have been estimated in mice,[1,4–6,9,12] rats,[11,12,14,17] rabbits, and pigs.[23–25] From these threshold studies, the pressure thresholds appear to be the same for mice, rats, and rabbits; pressure thresholds do not appear different as a function of frequency or beam width for mice and rats; pressure thresholds have a significant pulse duration (PD) trend for rats; and virtually every pressure threshold (normalized to the mechanical index [MI]) is less than the US Food and Drug Administration (FDA) regulatory limit (MI < 1.9[26]).

Also, at superthreshold exposure conditions (in situ [at the pleural surface] peak rarefactional pressure, $p_{r(in\ situ)}$, = 6.1 MPa), a 3 × 3 factorial design study (pulse repetition frequency [PRF]: 17, 170, and 1700 Hz; exposure duration [ED]: 5, 31.6, and 200 s) showed that the main effects of PRF and ED were not significant for lesion occurrence and sizes, whereas the interaction term (PRF × ED; total number of pulses) was highly significant.[18] These findings do not suggest, however, that PRF and ED did not have an effect. Rather, if either PRF or ED is held relatively constant, or varied over only a narrow range, then the number of pulses will appear as an effect of the nonconstant variable. These findings are consistent with those[1] that showed a slightly larger proportion of mice with lesions for 100-Hz PRF compared to 10-Hz PRF.

In general, however, the effect of exposure timing quantities (PD, ED, and PRF) on the threshold for ultrasound-induced lung hemorrhage and on the size of the lesions at superthreshold levels has been examined only to a limited extent. So far, only the interaction of PRF and ED has been examined. The interaction of PRF and PD has not been examined and thus is the purpose of this study for which the interaction term (PRF × PD) is the duty factor, the fractional amount of time the pulse is excited. Furthermore, this factorial PRF × PD study is an adjunct to the previously reported PD threshold study for which the PRF was held constant.[17]

Materials and Methods

Exposimetry

The exposimetry and calibration procedures have been described previously in considerable detail.[12,17] A focused, 19-mm-diameter, lithium niobate ultrasonic transducer (Valpey Fisher, Hopkinton, MA) was used. Water-based (degassed water, 22 ± 0.5°C) pulse-echo ultrasonic field distribution measurements were performed according to established procedures[12,27] and yielded a center frequency of 2.8 MHz, a fractional bandwidth of 12%, a focal length of 19 mm, a –6-dB focal beam width of 470 µm, and a –6-dB depth of focus of 2.7 mm.

An automated procedure routinely calibrated the ultrasound fields[12,17,28,29] and was based on established standards.[28,30] Briefly, the source transducer was mounted in a water tank (degassed water, 22 ± 0.5°C), and its drive voltage was supplied by a RAM5000 ultrasound system (Ritec, Inc, Warwick, RI). A calibrated polyvinylidene difluoride membrane hydrophone (model Y-34-6543; Marconi, Chelmsford, England), mounted to a computer-controlled micropositioning system (Daedal, Inc, Harrisburg, PA), scanned the ultrasound field along the determined beam axis. The hydrophone's signal was digitized with an oscilloscope (500 MS/s; model 9354TM; LeCroy, Chestnut Ridge, NY) and transferred to the same computer (Dell Pentium II; Dell Corporation, Round Rock, TX) that controlled the positioning system. The radio frequency data were transferred to a workstation and analyzed. Off-line processing (MATLAB; The Mathworks, Natick, MA) yielded the water-based peak rarefactional pressure [$p_{r(in\ vitro)}$] and the water-based peak compressional pressure [$p_{c(in\ vitro)}$]. The MI was also determined.[30] The purpose for providing the MI is because it is a regulated quantity[26] of diagnostic ultrasound systems, and its magnitude is available to system operators.

A total of 25 independent water-based calibrations of the 2.8-MHz transducer were conducted before, during, and after the 5-month period of the experiments; this study was conducted immediately after the PD threshold study[17] because the same PD-dependent calibration procedures were used. A set of in vitro pressure waveforms are shown in Figure 1. At the exposure levels used in this study, the relative SDs (SD × 100/mean) were 17% for $p_{r(in\ vitro)}$ and 20% for $p_{c(in\ vitro)}$.

The experimental protocol required the same $p_{r(in\ situ)}$ for all exposed animals. Rat chest wall insertion losses and thicknesses were used from previous experiments[11,12,17,31,32] to estimate the $p_{r(in\ vitro)}$ values that would correspond to the same $p_{r(in\ situ)}$ value. The actual $p_{r(in\ situ)}$ values obtained in this study were determined from the measured chest wall thicknesses (4.31 ± 0.13 mm) of the animals used herein, and the chest wall insertion loss (2.8 dB/cm at 2.8 MHz) was that previously determined.[31,32] The calculated $p_{r(in\ situ)}$ value ranged between 5.84 and 5.95 MPa. Thus, a $p_{r(in\ situ)}$ value of 5.9 MPa was used for the study protocol (Table 1).

Animals

The experimental protocol was approved by the Institutional Animal Care and Use Committee at the University of Illinois at Urbana-Champaign and satisfied all campus and National Institutes of Health rules for the humane use of laboratory

animals. Rats were housed in an animal facility approved by the Association for Assessment and Accreditation of Laboratory Animal Care (Rockville, MD), placed in groups of 1 to 3 in polycarbonate cages with Beta Chip bedding (NEPCO, Warrensburg, NY) and wire bar lids, and provided food and water ad libitum. The Association for Assessment and Accreditation of Laboratory Animal Care is a private nonprofit organization that promotes the humane treatment of animals in science through a voluntary accreditation program.

One hundred seventy-five 10- to 11-week-old 258 ± 13-g (mean ± SD) female Sprague Dawley rats (Harlan, Indianapolis, IN) were randomly divided into 16 ultrasonically exposed groups (10 rats per group) and 1 sham group (15 rats); no lesions were produced in the sham group. The experiment was a 4 × 4 factorial design with 4 PRF groups (50, 170, 500, and 1700 Hz) and 4 PD groups (1.3, 4.4, 8.2, and 11.6 μs); the PDs used herein were the same as those used for the PD threshold study.[17] The value was approximately the same (5.9 MPa) for all ultrasonically exposed groups. The individuals involved in animal handling, exposure, and lesion scoring were blinded to the exposure condition. The exposure conditions for each animal were revealed only after the final results were tabulated.

Rats were weighed and then anesthetized with ketamine hydrochloride (87.0 mg/kg) and xylazine (13.0 mg/kg) administered intraperitoneally. For each rat, the skin of the left thorax was exposed by removing the hair with an electric clipper, followed by a depilatory agent (Nair; Carter-Wallace, Inc, New York, NY) to maximize sound transmission. A black dot was placed on the skin between the ribs at approximately the sixth to ninth rib to guide the positioning of the ultrasonic beam. The anesthetized rat was placed in a specially designed holder. The ultrasonic transducer was attached to the holder. A removable pointer, attached to the transducer, was used to position the ultrasonic beam perpendicular to the skin at the position of the black dot with the beam's focal region approximately at the lung surface.[11,12,17]

The holder with the animal and mounted transducer was placed in degassed, temperature-controlled (30 ± 0.5°C) water. The low-power pulse-echo capability of the exposure system (RAM5000) displayed on an oscilloscope was used to adjust the axial center of the focal region to within 1 mm of the lung surface; this exposure condition was the sham exposure (Table 1). The PRF was 10 Hz, and the PD was 1.3 μs during the alignment procedure. All ultrasonically exposed animals received the same $p_{r(\text{in situ})}$ of 5.9 MPa. Pulse repetition frequency (17, 170, 500, and 1700 Hz) and PD (1.3, 4.4, 8.2, and 11.6 μs) were randomly assigned to each animal. During exposure, each rat was observed for changes in its breathing pattern and respiratory rate; no changes were observed by the on-site veterinarian. After exposure, the rat was removed from the water and holder and then euthanized under anesthesia by cervical dislocation.

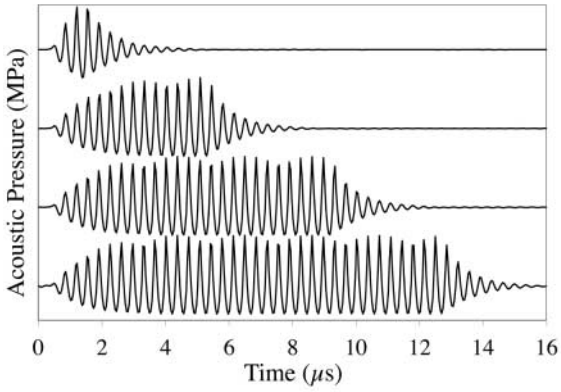

Figure 1. Temporal-dependent acoustic pressure waveforms of the 4 PDs. From top to bottom, the PDs are 1.3, 4.4, 8.2, and 11.6 μs. The in vitro peak rarefactional pressure for all waveforms is 6.8 MPa.

Table 1. Mean Values of the In Vitro (in Water) and In Situ (at the Pleural Surface) Peak Rarefactional and Peak Compressional Pressures

Parameter	Sham	Expose
$p_{r(\text{in vitro})}$, MPa	0.30	6.8 ± 0.04
$p_{c(\text{in vitro})}$, MPa	0.35	8.1 ± 0.25*
$p_{r(\text{in situ})}$, MPa	0.26 ± 0.001	5.9 ± 0.04
$p_{c(\text{in situ})}$, MPa	0.31 ± 0.001	7.0 ± 0.22†
MI	0.14	3.2 ± 0.02

The sham exposure conditions used a PRF of 10 Hz and a PD of 1.3 μs. The SD values for the in situ conditions represent the chest wall thickness variations. The SD values for the in vitro conditions resulted from the different PDs. The MI is provided because this is a regulated quantity of diagnostic ultrasound equipment.[26]

*Values were 7.6 MPa for the 1.3-μs PD and 8.2 MPa for the other 3 PDs.

†Values were 6.6 MPa for the 1.3-μs PD and 7.1 MPa for the other 3 PDs.

The thorax was opened, and the thickness of each left thoracic wall (skin, rib cage, and parietal pleura) at the point of exposure was measured with a digital micrometer (accuracy, 10 μm; Mitutoyo Corp, Kawasaki, Kanagawa, Japan). These chest wall measurements were used for later calculation of the in situ ultrasonic pressures at the visceral pleural surface. The lungs were removed from each rat, and the left lung lobe was scored for the presence or absence of hemorrhage. The left lung was fixed by immersion in 10% neutral-buffered formalin until the tissue was adequately fixed.[33] Although satisfactory fixation can be obtained in 24 hours, the fixation period was greater than 1 week. After fixation, the elliptical dimensions of each lung lesion at the visceral pleural surface were measured with a digital micrometer in which "a" was the semimajor axis and "b" was the semiminor axis. The surface area (πab) of the lesion was calculated for each animal. The lesion was then bisected, and the depth "d" of the lesion within the pulmonary parenchyma was also measured. Each half of the bisected lesion was embedded in paraffin, sectioned at 5 μm, stained with hematoxylin and eosin, and evaluated microscopically.

Statistics

Our primary interests were to model the effects of PRF and PD on lesion occurrence, depth, and surface area in exposed lungs. Logistic regression analysis and Gaussian tobit analysis were used to assess the significance of PRF and PD on the occurrence and size of lesions as previously described.[15,17,18,20,25] All statistical calculations were performed using the R statistical software package.[34]

The logistic regression models were estimated from occurrence data using the R function "glm," which calculated maximum likelihood estimates, SEs, and model statistics.[35] Let n_{ij} denote the number of animals with pulse duration PD_i and pulse repetition frequency PRF_j, and let Y_{ij} denote the number of animals exhibiting lesions at the combination of PD_i and PRF_j. Furthermore, assume π_{ij} is the probability of a lesion for PD_i and PRF_j. As is well known, Y_{ij} is then binomially distributed with the number of trials and event probability π_{ij}. The full (saturated) model has the form

$$(1) \qquad \log\left(\frac{\pi_{ij}}{1-\pi_{ij}}\right) = \alpha + \beta_i^{PD} + \beta_j^{PRF} + \gamma_{ij}^{PD\times PRF},$$

for $i = 1, \ldots, 4$ and $j = 1, \ldots, 4$, where α is the intercept; β_i^{PD} is the main effect for PD; β_j^{PRF} is the main effect for PRF; $\gamma_{ij}^{PD\times PRF}$ is the interaction parameter; and $(i = 1, j = 1)$ is used as the reference cell in the design for the saturated model (Equation 1) such that

$$\beta_1^{PD} = \beta_1^{PRF} = \gamma_{1j}^{PD\times PRF} = \gamma_{i1}^{PD\times PRF} = 0.$$

Each of the coefficients represents an increment in the log-odds of a lesion compared with the reference exposure of $PD_1 = 1.3$ μs and $PRF_1 = 50$ Hz.

To reduce the complexity of the saturated model (Equation 1), trend models were also considered, in which the log-odds depend linearly on numerical values of PD (in μs), PRF (in kHz), and their product, that is,

$$(2) \qquad \log\left(\frac{\pi_{ij}}{1-\pi_{ij}}\right) = \beta_o + \beta_1 PD_i + \beta_2 PRF_j + \gamma_{12} PD_i \times PRF_j,$$

where β_0 is the intercept; β_1 is the PD coefficient; β_2 is the PRF coefficient; and γ_{12} is the interaction coefficient. A likelihood ratio test for the trend model (Equation 2) versus the saturated model (Equation 1) provided a goodness-of-fit test of the reduced full-trend model.[36] χ^2 tests of the coefficients in the full-trend model (Equation 2) were used to determine statistical significance of PD, PRF, and the interaction term.

Data on lesion depth and root surface area ($\sqrt{\text{surface area}}$; the square root transformation was used to make the surface area data close to being normally distributed) were analyzed by Gaussian tobit regression.[37] The computations were performed using the "survreg" function in R.[38] Tobit regression is a model for nonnegative-valued responses with a threshold at 0. If the lung shows a lesion, then the response is the measured depth (or root surface area) of the lesion. If no lesion is present, then the depth is 0. Let Z_{ijk} denote the depth (or root surface area) for the kth animal (10 in total) with $PD = PD_i$ and $PRF = PRF_j$. The tobit regression model entails that Z_{ijk} has a normal distribution censored below at 0. Let μ_{ij} denote the mean of the uncensored normal distribution for PD_i and PRF_j, and let σ^2 denote its variance. If μ_{ij} is positive, then μ_{ij} is also the median lesion size (depth or square root surface area); whereas if μ_{ij} is negative, then the median lesion size is 0. The saturated model for lesion size specifies that

$$(3) \qquad \mu_{ij} = \alpha + \beta_i^{PD} + \beta_j^{PRF} + \gamma_{ij}^{PD\times PRF},$$

where the coefficients satisfy the same constraints as in the logistic regression model (Equation 1). The trend model has the form

$$(4) \quad \mu_{ij} = \beta_o + \beta_1 PD_i + \beta_2 PRF_j + \gamma_{12} PD_i \times PRF_j ,$$

where the coefficients and variables are defined in the same way as in the logistic regression trend model (Equation 2). The tobit models were fit by the method of maximum likelihood using the "survreg" function in R,[38] and medians and 75th percentiles of lesion depth and surface area were computed from the final models for each combination of PD and PRF.

Results

The PRF and PD data for ultrasound-induced lung hemorrhage are shown in Figure 2.

For the logistic regression on lesion occurrence, the likelihood ratio test of the trend model (Equation 2) versus the saturated model (Equation 1) was not significant ($P = .17$), indicating that the trend model was sufficient to model the data. Furthermore, the main effect of PRF in the full-trend model (Equation 2) was not significant ($P > .4$); therefore, a simplified trend model depending only on the main effect of PD and the interaction PRF × PD was sufficient. Table 2 provides a summary of the final logistic regression trend model, including coefficient estimates, SEs, χ^2 values, and P values for tests that the corresponding coefficients are 0. The interaction term, PRF × PD, was highly significant in the simplified trend model, indicating a strong positive dependence of lesion occurrence on duty factor. The main effect of PD was nearly significant ($P = .052$) and was included in the final simplified trend model to ensure an adequate model fit for risk estimation. The observed proportions and estimated probabilities of lesions at all combinations of PD and PRF are given in Table 3. Figure 3 shows the observed proportions of lesions and estimated probabilities as increasing functions of PRF × PD.

Hence, the probability of a lesion is positively associated with both the PD main effect and the product term PRF × PD, with the latter being the major term that affected lesion occurrence. Figure 4 provides the 4 fitted lines for log-odds of a lesion as a function of PRF (in kHz) conditional on each of the 4 PD levels. Given any PD value, that is, within each fitted line, the log-odds of a lesion is an increasing function of PRF. While for

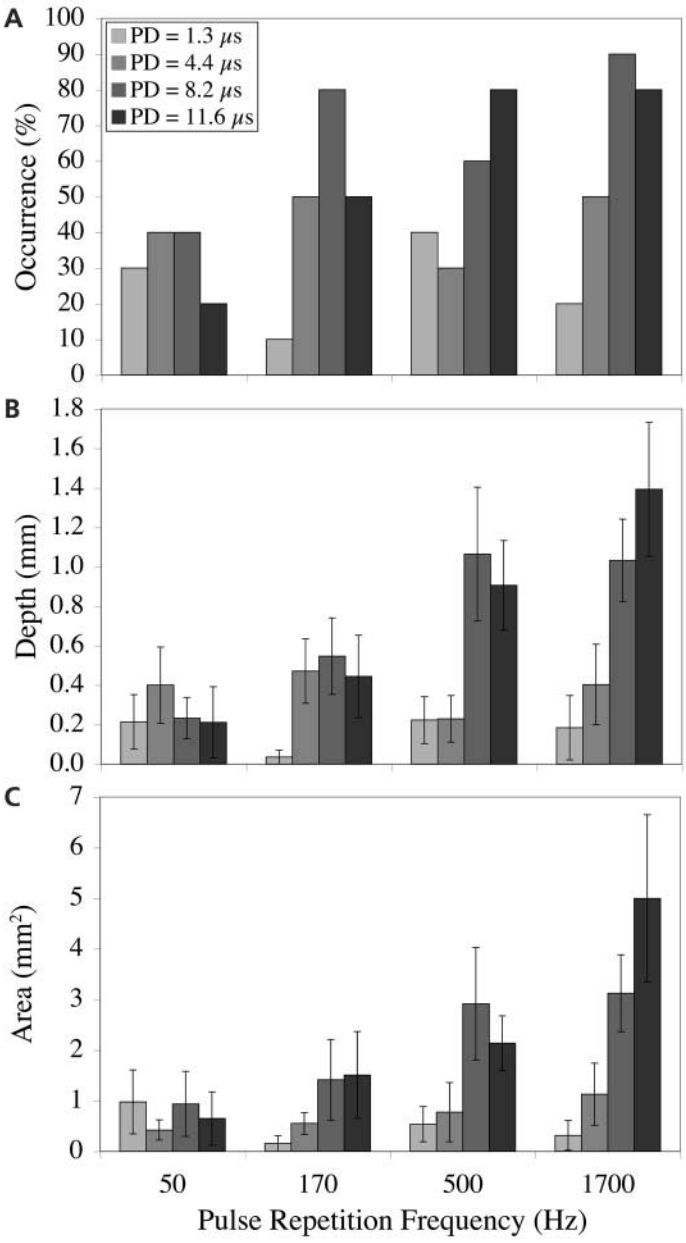

Figure 2. Mean lesion occurrence (**A**), depth (**B**), and surface area (**C**) in rats as a function of PRF for 4 PDs. Error bars represent SEM.

Table 2. Logistic Regression Model for Occurrence of Lesions

Variable	Coefficient	SE	χ^2	*df*	*P*
Intercept	–1.068	0.330	10.472	1	.0012
PD	0.092	0.047	3.787	1	.0517
PD × PRF	0.116	0.042	7.508	1	.0061

Table 3. Observed Proportions of Lesions and Probability Estimates (in Parentheses) Based on Logistic Regression Model

Variable	PRF = 50 Hz	PRF = 170 Hz	PRF = 500 Hz	PRF = 1700 Hz
PD = 1.3 μs	0.3 (0.281)	0.1 (0.284)	0.4 (0.294)	0.2 (0.333)
PD = 4.4 μs	0.4 (0.345)	0.5 (0.359)	0.3 (0.399)	0.5 (0.550)
PD = 8.2 μs	0.4 (0.433)	0.8 (0.461)	0.6 (0.539)	0.9 (0.785)
PD = 11.6 μs	0.2 (0.515)	0.5 (0.555)	0.8 (0.660)	0.8 (0.907)

Figure 3. A, Observed proportions of lesions and estimated (fitted) probabilities of lesions based on the logistic regression model. **B**, Seventy-fifth percentile of lesion depth based on sample percentiles (observed) and model based-percentiles (fitted). **C**, Seventy-fifth percentile of the square root of lesion surface area based on sample percentiles (observed) and model-based percentiles (fitted) as a function of duty factor (PRF in Hz, PD in s, and log displayed). For example, a log duty factor of –3 is 10^{-3} or 0.001.

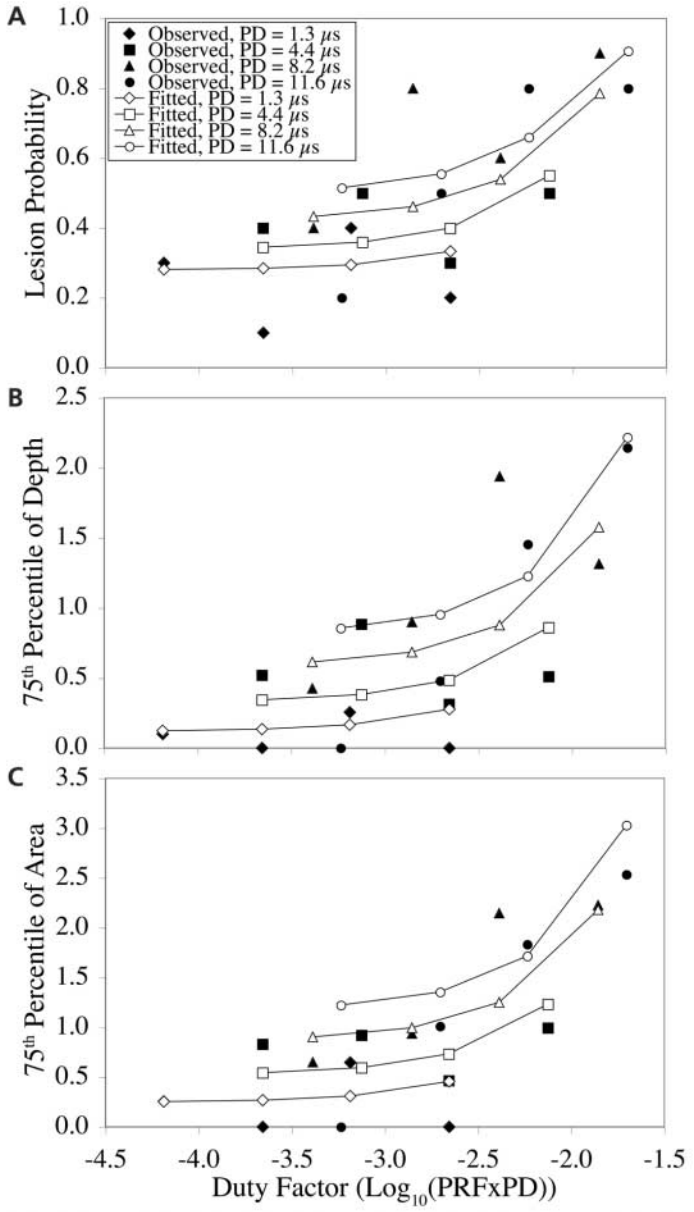

different PD levels, the fitted lines have different intercepts and slopes: as PD increases, the intercept (background log-odds of lesion provided PRF = 0) and slope (change in log-odds of a lesion when PRF varies 1 unit) both increase. Note that the slope for PD = 1.3 μs is relatively flat and that for PD = 11.6 μs is much steeper, which indicates a slow increase in probability of a lesion as PRF increases when PD is short and a quick increase of lesion occurrence as PRF goes up when PD is relatively long. Figure 5 shows the 4 fitted lines for log-odds of a lesion as a function of PD (in μs) conditional on PRF. Similarly, the fitted log-odds of a lesion is an increasing function of PD given PRF. As the main effect of PRF is not significant, the 4 fitted lines have different slopes but the same intercept.

The analogous tobit models were fit to the data on lesion depth and square root surface area. The final simplified trend models are summarized in Tables 4 and 5. Similar to the results for lesion occurrence data, lesion depth and surface area also depend significantly on the main effect of PD ($P = .02$) and PRF × PD ($P < .001$), and the median lesion size exhibits a strong positive dependence on duty factor. Compared with logistic regression of occurrence, these models have an extra parameter (σ) to model the variation about the median lesion size. Tables 6 and 7 show sample 75th percentiles and 75th percentiles computed from the final tobit regression models for each combination of PRF and ED. These sample percentiles and model-based percentiles are plotted in Figure 3 to show the positive dependence between lesion size and duty factor.

Figure 4. Estimated log-odds of a lesion based on logistic regression of lesion occurrence showing the dependence on PRF for 4 PDs.

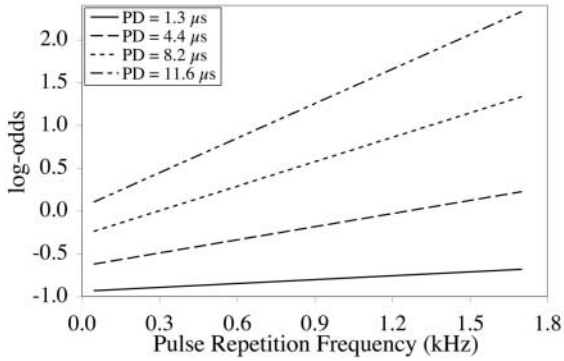

Discussion

The primary result of the 4 × 4 factorial analysis on rats is the statistically significant positive dependence of lesion occurrence and size on the interaction between PRF and PD as well as the main effect of PD, in other words, on the fraction of time that the ultrasound pulses are on and a single PD. The fraction of "on" time (duty factor) is the major effect. Overall, the trends for lesion depth and surface area are parallel with the probability trends in the logistic regression analysis of lesion occurrence.

In our previous 3 × 3 factorial analysis on rats for which the interaction between PRF and ED was evaluated, $p_{r(\text{in situ})}$ of 6.1 MPa was used[18] because an earlier PRF × ED study[11] resulted in saturation of the results (for which $p_{r(\text{in situ})}$ was 12.3 MPa). To minimize the possibility of saturation in this 4 × 4 factorial, PRF × PD study, $p_{r(\text{in situ})}$ of 5.9 MPa was used.

The 500- and 1700-Hz PRF results agree well with the PD threshold results.[17] The PD threshold study used a PRF of 1000 Hz; thus, the 500- and 1700-Hz PRFs bracketed the PD threshold study; ED of 10 s and the 4 PDs were the same for both studies. The 500- and 1700-Hz PRF results for the 4 PDs fall within the range of those results of the PD threshold study at a $p_{r(\text{in situ})}$ of 5.9 MPa (Figure 6). Also, this value is in the range of the ED_{50} values in the PD threshold study,[17] for which, at a PRF of 1000 Hz, the ED_{50} occurrence estimates monotonically decrease from 6.7 MPa (for 1.3-µs PD) to 5.5 MPa (for 11.6-µs PD).

The $p_{r(\text{in situ})}$ value of 5.9 MPa at a frequency of 2.8 MHz is greater than that allowed by the FDA.[26] The measured MI was 3.24 ± 0.02, whereas the FDA's limit is 1.9. The purpose of selecting this exposure level was to study the biophysical response, thus requiring a level that would ensure an effect. Other studies have experimentally estimated pressure thresholds,[1,4–6,9,11,12,14,17,23–25] and these thresholds are typically less than an MI of 1.9. However, the selection of PRF and PD falls within the clinical diagnostic range. Typical gray scale B-mode imaging uses PRFs in the range of 500 to 2000 Hz, and blood flow measurements use PDs in the range of about 1 to 8 µs.

Table 4. Summary of Tobit Model for Lesion Depth

Variable	Coefficient	SE	χ^2	*df*	*P*
Intercept	–0.698	0.215	10.517	1	.0012
PD	0.068	0.028	5.655	1	.0174
PD × PRF	0.071	0.019	14.631	1	.0001
log(σ)	0.078	0.090	0.752	1	.3858

Table 5. Summary of Tobit Model for Square Root Lesion Surface Area

Variable	Coefficient	SE	χ^2	*df*	*P*
Intercept	–0.857	0.290	8.703	1	.0032
PD	0.089	0.038	5.429	1	.0198
PD × PRF	0.095	0.025	14.063	1	.0002
log(σ)	0.381	0.091	17.724	1	<.0001

Active variables are PRF (in kHz) and PD (in µs).

Table 6. Sample and Model-Based 75th Percentiles (in Parentheses) for Lesion Depth (mm)

Variable	PRF = 50 Hz	PRF = 170 Hz	PRF = 500 Hz	PRF = 1700 Hz
PD = 1.3 µs	0.100 (0.123)	0.000 (0.134)	0.255 (0.165)	0.000 (0.276)
PD = 4.4 µs	0.520 (0.344)	0.885 (0.381)	0.315 (0.485)	0.510 (0.861)
PD = 8.2 µs	0.425 (0.614)	0.900 (0.684)	1.940 (0.877)	1.315 (1.577)
PD = 11.6 µs	0.000 (0.856)	0.480 (0.955)	1.455 (1.228)	2.145 (2.218)

Table 7. Sample and Model-Based 75th Percentiles (in Parentheses) for Root Lesion Surface Area (mm^2)

Variable	PRF = 50 Hz	PRF = 170 Hz	PRF = 500 Hz	PRF = 1700 Hz
PD = 1.3 µs	0.255 (0.253)	0.000 (0.268)	0.648 (0.308)	0.000 (0.456)
PD = 4.4 µs	0.831 (0.544)	0.920 (0.594)	0.464 (0.732)	0.994 (1.231)
PD = 8.2 µs	0.649 (0.902)	0.938 (0.995)	2.147 (1.251)	2.227 (2.181)
PD = 11.6 µs	0.000 (1.222)	1.010 (1.354)	1.833 (1.715)	2.536 (3.031)

Figure 5. Estimated log-odds of a lesion based on logistic regression of lesion occurrence showing the dependence on PD for 4 PRFs.

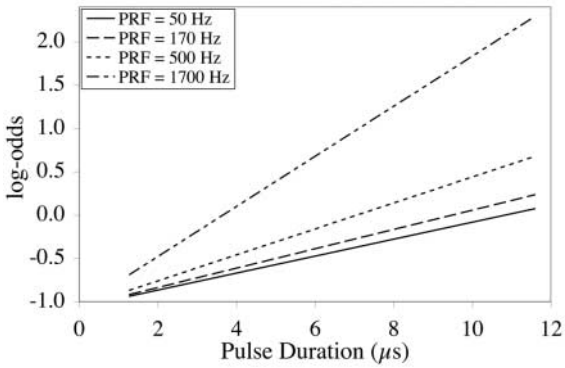

In comparing the results of this article with previous results, the lack of main effects for PRF does not necessarily suggest that this variable has no effect, rather that the strongest effects are the PD and the duty factor (PRF × PD). If PRF is held constant, as it was for the PD threshold study at 1000 Hz,[17] then the duty factor might appear as an effect of the nonconstant variable. However, when comparing the ED_{50} occurrence and size estimates in the PD threshold study, the 2 most extreme PDs (1.3 and 11.6 μs) were nonoverlapping even though the downward trend of the ED_{50} occurrence (upward trend in the occurrence probability of a lesion) as the PD increased was significant despite the uncertainty in estimating the ED_{50} thresholds. This thus suggests that the PD is also a weak effect, an observation consistent with the statistical model. Also, our results do not appear to be consistent with those[1] that reported in mice that there was no duty factor effect when comparing 100-Hz PRF with 1000-Hz PRF (PD constant at 10 μs); however, given the weak PRF effect reported herein, their reported result may be due to the fact that only PRF was changed.

On the basis of our previous 3 × 3 factorial, PRF × ED study, we suggested that the MI definition may need to consider the number of pulses (product of PRF and ED) rather than the individual variables.[18] Our current 4 × 4 factorial, PRF × PD study supports this view, namely, the MI definition may need to consider a combination (possibly product) of individual variables rather than the individual variables. Duty factor, the product of PRF and PD, has been shown to be statistically significant for lesion occurrence and size. Likewise, a similar finding was shown to be statistically significant for the product of PRF and ED.[25] Perhaps a function that considers PRF, PD, and ED might yield a sensitive indicator for a modified MI, but the experiment to determine this has not yet been performed. Furthermore, because of the consistent frequency-independent ultrasound-induced lung hemorrhage findings (frequency is included in the MI determination), it is suggested that a new index for diagnostic ultrasound regulatory purposes be considered to quantify nonthermal mechanisms, at least for the lung.

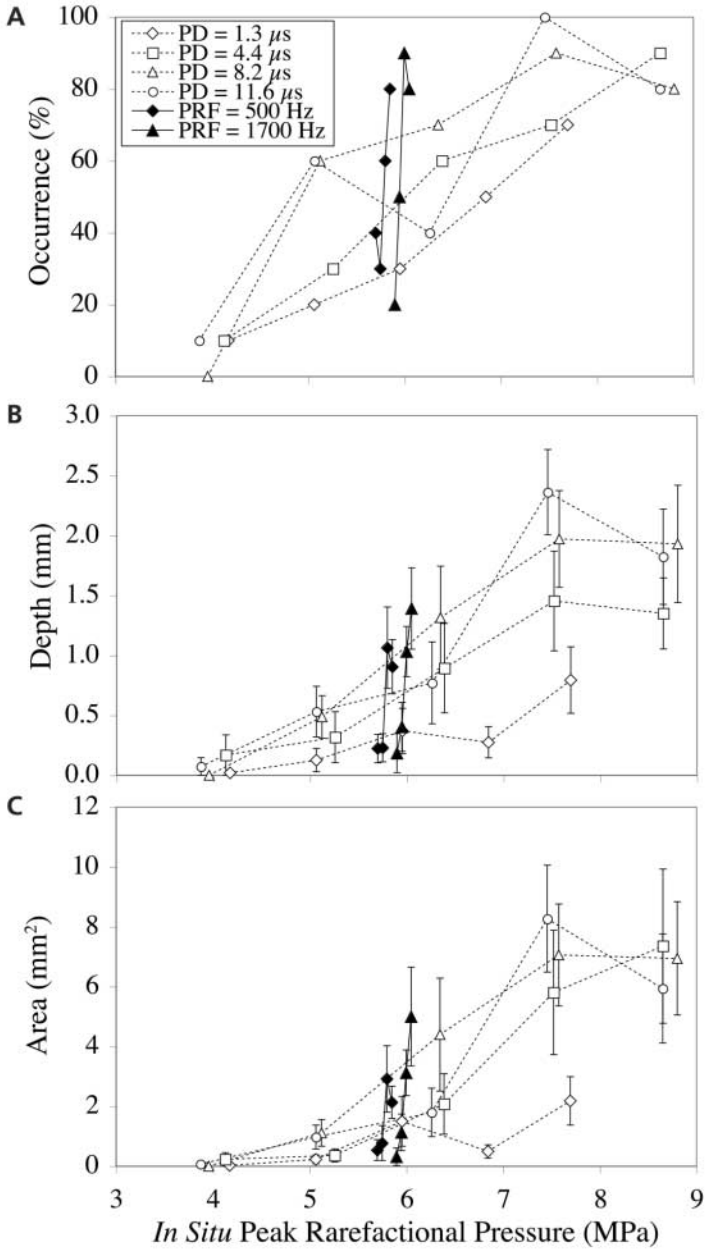

Figure 6. Comparison of mean lesion occurrence (**A**), depth (**B**), and surface area (**C**) in rats as a function of $p_{r(in\ situ)}$. The open symbol data points connected by dashed lines represent the PD threshold study[17] for the 4 PDs (the PRF was 1000 Hz). The solid symbol data points connected by solid lines represent the 500- and 1700-Hz PRF results reported herein [data points have been slightly shifted for graphical clarity around 5.9-MPa $p_{r(in\ situ)}$]; data points as connected from lower to higher values represent increasing PD. Error bars represent SEM.

References

1. Child SZ, Hartman CL, Schery LA, Carstensen EL. Lung damage from exposure to pulsed ultrasound. Ultrasound Med Biol 1990; 16:817–825.

2. Hartman C, Child SZ, Mayer R, Schenk E, Carstensen EL. Lung damage from exposure to the fields of an electrohydraulic lithotripter. Ultrasound Med Biol 1990; 16:675–683.

3. Penney DP, Schenk EA, Maltby K, Hartman-Raeman C, Child SZ, Carstensen EL. Morphologic effects of pulsed ultrasound in the lung. Ultrasound Med Biol 1993; 19: 127– 135.

4. Raeman CH, Child SZ, Carstensen EL. Timing of exposures in ultrasonic hemorrhage of murine lung. Ultrasound Med Biol 1993; 19:507–512.

5. Raeman CH, Child SZ, Dalecki D, Cox C, Carstensen EL. Exposure-time dependence of the threshold for ultrasonically induced murine lung hemorrhage. Ultrasound Med Biol 1996; 22:139–141.

6. Frizzell LA, Chen E, Lee C. Effects of pulsed ultrasound on the mouse neonate: hind limb paralysis and lung hemorrhage. Ultrasound Med Biol 1994; 20:53–63.

7. Zachary JF, O'Brien WD Jr. Lung lesion induced by continuous- and pulsed-wave (diagnostic) ultrasound in mice, rabbits, and pigs. Vet Pathol 1995; 32:43–45.

8. O'Brien WD Jr, Zachary JF. Lung damage assessment from exposure to pulsed-wave ultrasound in the rabbit, mouse, and pig. IEEE Trans Ultrason Ferroelectr Freq Control 1997; 44:473–485.

9. Dalecki D, Child SZ, Raeman CH, Cox C, Penney DP, Carstensen EL. Age dependence of ultrasonically induced lung hemorrhage in mice. Ultrasound Med Biol 1997; 23:767–776.

10. O'Brien WD Jr, Frizzell LA, Weigel RM, Zachary JF. Ultrasound-induced lung hemorrhage is not caused by inertial cavitation. J Acoust Soc Am 2000; 108:1290–1297.

11. O'Brien WD Jr, Frizzell LA, Schaeffer DJ, Zachary JF. Superthreshold behavior of ultrasound-induced lung hemorrhage in adult mice and rats: role of pulse repetition frequency and pulse duration. Ultrasound Med Biol 2001; 27:267–277.

12. Zachary JF, Sempsrott JM, Frizzell LA, Simpson DG, O'Brien WD Jr. Superthreshold behavior and threshold estimation of ultrasound-induced lung hemorrhage in adult mice and rats. IEEE Trans Ultrason Ferroelectr Freq Control 2001; 48:581–592.

13. Frizzell LA, O'Brien WD Jr, Zachary JF. Effect of pulse polarity and energy on ultrasound-induced lung hemorrhage in adult rats. J Acoust Soc Am 2003; 113:2912–2926.

14. Holland CK, Deng CX, Apfel RE, Alderman JL, Fenandez LA, Taylor KJW. Direct evidence of cavitation in vivo from diagnostic ultrasound. Ultrasound Med Biol 1996; 22: 917–925.

15. O'Brien WD Jr, Simpson DG, Frizzell LA, Zachary JF. Superthreshold behavior and threshold estimation of ultrasound-induced lung hemorrhage in adult rats: role of beamwidth. IEEE Trans Ultrason Ferroelectr Freq Control 2001; 48:1695–1705.

16. O'Brien WD Jr, Kramer JM, Waldrop TG, Frizzell LA, Zachary JF. Ultrasound-induced lung hemorrhage: role of acoustic boundary conditions at the pleural surface. J Acoust Soc Am 2002; 111:1102–1109.

17. O'Brien WD Jr, Simpson DG, Frizzell LA, Zachary JF. Threshold estimates and superthreshold behavior of ultrasound-induced lung hemorrhage in adult rats: role of pulse duration. Ultrasound Med Biol 2003; 29:1625–1634.

18. O'Brien WD Jr, Simpson DG, Frizzell LA, Zachary JF. Superthreshold behavior of ultrasound-induced lung hemorrhage in adult rats: role of pulse repetition frequency and exposure duration revisited. J Ultrasound Med 2005; 24: 339–348.

19. Kramer JM, Waldrop TG, Frizzell LA, Zachary JF, O'Brien WD Jr. Cardiopulmonary function in rats with lung hemorrhage induced by exposure to superthreshold pulsed ultrasound. J Ultrasound Med 2001; 20:1197–1206.

20. Zachary JF, Frizzell LA, Norrell KS, Blue JP Jr, Miller RJ, O'Brien WD Jr. Temporal and spatial evaluation of lesion resolution following exposure of rat lung to pulsed ultrasound. Ultrasound Med Biol 2001; 27:829–839.

21. Tarantal AF, Canfield DR. Ultrasound-induced lung hemorrhage in the monkey. Ultrasound Med Biol 1994; 20: 65–72.

22. Harrison GH, Eddy HA, Wang JP, Liberman FZ. Microscopic lung alterations and reduction of respiration rate in insonated anesthetized swine. Ultrasound Med Biol 1995; 21:981–983.

23. Baggs R, Penney DP, Cox C, et al. Thresholds for ultrasonically induced lung hemorrhage in neonatal swine. Ultrasound Med Biol 1996; 22:119–128.

24. Dalecki D, Child SZ, Raeman CH, Cox C, Carstensen EL. Ultrasonically induced lung hemorrhage in young swine. Ultrasound Med Biol 1997; 23:777–781.

25. O'Brien WD Jr, Simpson DG, Ho M-H, Miller RJ, Frizzell LA, Zachary JF. Superthreshold behavior and threshold estimation of ultrasound-induced lung hemorrhage in pigs: role of age dependency. IEEE Trans Ultrason Ferroelectr Freq Control 2003; 50:153–169.

26. US Food and Drug Administration. Information for Manufacturers Seeking Marketing Clearance of Diagnostic Ultrasound Systems and Transducers. Rockville, MD: Center for Devices and Radiological Health, US Food and Drug Administration; 1997.

27. Raum K, O'Brien WD Jr. Pulse-echo field distribution measurement technique of high-frequency ultrasound sources. IEEE Trans Ultrason Ferroelectr Freq Control 1997; 44:810–815.

28. American Institute of Ultrasound in Medicine, National Electrical Manufacturers Association. Acoustic Output Measurement Standard for Diagnostic Ultrasound Equipment. Laurel, MD: American Institute of Ultrasound in Medicine; Rosslyn, VA: National Electrical Manufacturers Association; 1998.

29. Sempsrott JM, O'Brien WD Jr. Experimental verification of acoustic saturation. In: Proceedings of the 1999 IEEE Ultrasonics Symposium. Piscataway, NJ: Institute of Electrical and Electronics Engineers; 1999:1287–1290.

30. American Institute of Ultrasound in Medicine, National Electrical Manufacturers Association. Output Display Standard: Standard for Real-Time Display of Thermal and Mechanical Acoustic Output Indices on Diagnostic Ultrasound Equipment. Rev 2. Laurel, MD: American Institute of Ultrasound in Medicine; Rosslyn, VA: National Electrical Manufacturers Association; 2004.

31. Teotico GA, Miller RJ, Frizzell LA, Zachary JF, O'Brien WD Jr. Attenuation coefficient estimates of mouse and rat chest wall. IEEE Trans Ultrason Ferroelectr Freq Control 2001; 48:593–601.

32. Towa RT, Miller RJ, Frizzell LA, Zachary JF, O'Brien WD Jr. Attenuation coefficient and propagation speed estimates of rat and pig intercostal tissue as a function of temperature. IEEE Trans Ultrason Ferroelectr Freq Control 2002; 49:1411–1420.

33. Sheehan DC, Hrapchak BB. Theory and Practice of Histological Techniques. 2nd ed. St Louis, MO: CV Mosby Co; 1980:44, 49.

34. Ihaka R, Gentleman R. R: a language for data analysis and graphics. J Comput Graph Stat 1996; 5:299–314.

35. Hosmer DW, Lemeshow S. Applied Logistic Regression. 2nd ed. New York, NY: John Wiley & Sons; 2000.

36. Agresti A. An Introduction to Categorical Data Analysis. New York, NY: John Wiley & Sons; 1996.

37. Amemiya T. Tobit models: a survey. J Econom 1984; 24:3–61.

38. Galfalvy H, Simpson DG. Infrastructure degradation: an application of censored regression models. In: American Statistical Association Proceedings of the Section on Physical and Engineering Sciences. Alexandria, VA: American Statistical Association; 1999:242–247.